Published in final edited form as:
Microsyst Technol. 2014 October 1; 20(10-11): 1815–1825. doi:10.1007/s00542-013-1941-6.

Arrays of High-Aspect Ratio Microchannels for High-Throughput Isolation of Circulating Tumor Cells (CTCs)

Mateusz L. Hupert[1,5,*], **Joshua M. Jackson**[2], **Hong Wang**[1], **Małgorzata A. Witek**[1], **Joyce Kamande**[3], **Matthew I. Milowsky**[4], **Young E. Whang**[4], and **Steven A. Soper**[1,2,4,5,*]

[1]Department of Biomedical Engineering, University of North Carolina, Chapel Hill, NC, USA

[2]Department of Chemistry, University of North Carolina, Chapel Hill, NC, USA

[3]Department of Chemistry, Louisiana State University, Baton Rouge, LA, USA

[4]Lineberger Comprehensive Cancer Center, UNC School of Medicine, Chapel Hill, NC, USA

[5]BioFluidica, Inc., Chapel Hill, NC, USA

Abstract

Microsystem-based technologies are providing new opportunities in the area of in vitro diagnostics due to their ability to provide process automation enabling point-of-care operation. As an example, microsystems used for the isolation and analysis of circulating tumor cells (CTCs) from complex, heterogeneous samples in an automated fashion with improved recoveries and selectivity are providing new opportunities for this important biomarker. Unfortunately, many of the existing microfluidic systems lack the throughput capabilities and/or are too expensive to manufacture to warrant their widespread use in clinical testing scenarios. Here, we describe a disposable, all-polymer, microfluidic system for the high-throughput (HT) isolation of CTCs directly from whole blood inputs. The device employs an array of high aspect ratio (HAR), parallel, sinusoidal microchannels (25 μm × 150 μm; W × D; AR = 6.0) with walls covalently decorated with anti-EpCAM antibodies to provide affinity-based isolation of CTCs. Channel width, which is similar to an average CTC diameter (12–25 μm), plays a critical role in maximizing the probability of cell/wall interactions and allows for achieving high CTC recovery. The extended channel depth allows for increased throughput at the optimized flow velocity (2 mm/s in a microchannel); maximizes cell recovery, and prevents clogging of the microfluidic channels during blood processing. Fluidic addressing of the microchannel array with a minimal device footprint is provided by large cross-sectional area feed and exit channels poised orthogonal to the network of the sinusoidal capillary channels (so-called Z-geometry). Computational modeling was used to confirm uniform addressing of the channels in the isolation bed. Devices with various numbers of parallel microchannels ranging from 50 to 320 have been successfully constructed. Cyclic olefin copolymer (COC) was chosen as the substrate material due to its superior properties during UV-activation of the HAR microchannels surfaces prior to antibody attachment. Operation of the HT-CTC device has been validated by isolation of CTCs directly from blood secured from patients with metastatic prostate cancer. High CTC sample purities (low

*corresponding authors: mhupert@med.unc.edu; +1 919-843-7835; and ssoper@unc.edu; +1-919-845-5585.

The authors declare the following competing financial interest(s): M.L.H. and S.A.S. have financial interests in BioFluidica, Inc.

number of contaminating white blood cells, WBCs) allowed for direct lysis and molecular profiling of isolated CTCs.

1. Introduction

Deaths from cancer typically result from metastatic disease; in fact, 90% of all cancer-related deaths result from metastatic disease. For most solid tumors, metastasis arises from the release of cancer cells entering into circulation (circulating tumor cells, CTCs). The resultant CTCs are thought to reflect the genetic and phenotypic diversity of the tumor and evolve in a manner reflecting the progression from the primary to metastasis (Hou et al. 2010). They can be found in most patients with solid tumors using current isolation methods (Allard et al. 2004). However, patients with more advanced disease have a higher CTC number (Nakagawa et al. 2007). CTCs in breast cancer patients are present in the blood in numbers that range from one to hundreds per mL (Yang et al. 2009), yet elevated leukocyte counts into the isolated fractions (*i.e.,* low purity) may preclude securing high quality molecular data from these CTC fractions (Smirnov et al. 2005; Maheswaran and Haber 2010; Farace et al. 2011).

The main challenge associated with the analysis of CTCs is their low frequency in a high background of spectator cells (*i.e.,* hematopoietic cells). Highly sensitive and specific enrichment techniques are required to enable effective CTC clinical analysis, especially molecular analysis. Three important metrics are considered when evaluating CTC enrichment techniques; (i) throughput, defined as the maximum volume processing rate; (ii) recovery, an indicator of the number of target cells selected from the input sample with respect to the seed level of the target in that same sample; and (iii) purity defined as the ratio of CTCs selected to the total number of cells enriched.

Johnson and Johnson's Veridex CellSearch™ is an FDA 510K cleared technology for CTC enrichment. It has begun clinical trials in breast, prostate and colorectal cancers, although it is not yet part of any conventional treatment or diagnostic protocol. The CellSearch™ system uses functionalized immunomagnetic beads that target the tumor specific antigen, epithelial cell adhesion molecule (EpCAM), often associated with CTCs. The CellSearch™ system has been publicized and validated for clinical trial purposes, yet low purity (0.01–0.1%) and poor clinical sensitivity are known inadequacies. Recent data has shown that 7/9 normal-type breast cancer cell lines could not be recovered using the CellSearch system (Sieuwerts et al. 2009; Mostert et al. 2011). In addition sample pre-processing steps are laborious and lengthy, generating long assay turnaround times. Furthermore, assay kit costs are very high. Thus, new, more efficient, and less expensive technologies that can provide similar or higher CTC sensitivity and specificity will be competitive in the medical device marketplace.

CellSearch typically recovers fewer CTCs from clinical samples than newer platforms, such as those based on microfluidics, which can directly process whole blood and isolate CTCs with high recovery (Kuo et al. 2010; Lin et al. 2009; Dharmasiri et al. 2010; Maheswaran et al. 2008; Xu et al. 2009; Adams et al. 2008; Tan et al. 2009; Nagrath et al. 2007; Dharmasiri et al. 2009). Microfluidic devices are attractive platforms for the analysis of CTCs for

several reasons: (i) They can be configured to select CTCs based on several different modalities including biological cell properties, such as expression of antigens specific to the CTC type, or physical cell properties, such as size (Williams et al. 2012). (ii) Microfluidic devices operate in a closed architecture, minimizing the potential of sample contamination artifacts that may provide false positive results, especially in clinical laboratory settings. (iii) Microfluidic devices can be produced in a high production mode and at low-cost. For example, devices can be produced in thermoplastics using micro-replication, the same technology used to produce consumables such as CD and DVDs (Adams et al. 2008; Dharmasiri et al. 2009; Dharmasiri et al. 2011). (iv) CTC selection devices can be integrated to other processing steps to fully automate sample processing, negating the need for operator intervention and thus, minimizing false negative results.

Microfluidic devices using affinity-based assays typically demonstrate higher purities compared to those based on size differences between the CTCs and blood cells but at the expense of throughput (Adams et al. 2008; Nagrath et al. 2007; Saliba et al. 2010; Dharmasiri et al. 2011). CTC affinity beds in microfluidic platforms have employed a variety of geometrical configurations (e.g. arrays of microposts, high aspect ratio microchannels, nanotextured channels, herringbone designs) to optimize recoveries (Adams et al. 2008; Dharmasiri et al. 2011; Nagrath et al. 2007). A CTC chip utilizing a staggered arrangement of microposts produced a recovery of 65% at low shear (0.4 dynes/cm^2) with a throughput of 1 mL/h (Nagrath et al. 2007), while herringbone channels are found to induce chaotic mixing leading to recoveries on the order of 91% and purities from 9% to 14% (Stott et al. 2010). Recently, a nanotextured herringbone device consisting of silicon nanopillars poised on a fluidic channel was reported (Wang et al. 2011). A flow rate of 1 mL/h was used for CTC selection from clinical samples. Adams and coworkers utilized sinusoidal high aspect ratio microchannels to reduce pressure drops and improved throughput for positive selection (1.6 mL/h). A recovery of MCF 7 cells spiked into blood was reported to be 97% (Adams et al. 2008).

Herein, we demonstrate a novel high-throughput (HT) CTC isolation device consisted of a parallel array of high aspect ratio (HAR) sinusoidal microchannels with nominal dimensions of 25 μm × 150 μm × 30 mm arranged in a Z-configuration. The high aspect ratio of the microchannels allowed short assay times for processing blood samples while maintaining the optimum average fluid velocity of 2 mm/s for maximum recovery and at a CTC capture-enhancing channel width of 25 μm. The Z-type arrangement of the inlet and outlet channels occupied a smaller footprint compared to our previously reported CTC capture device (Adams et al. 2008; Dharmasiri et al. 2011), allowed for uniform addressing of parallel microchannels, and easy scaling of the CTC isolation bed to accommodate larger number of microchannels to further increase device throughput. Furthermore, it improved the control of HT-CTC device operation by providing high linear fluid velocities in the inlet and outlet channels, which efficiently removed persistent air bubbles that are inevitably introduced into device architectures during operation. We present the results of the fabrication and characterization of the HT-CTC chips in polymers via hot-embossing and discuss our studies on proper material selection for chip construction with respect to the efficiency of antibody attachment to the microchannel surface. Finally, we demonstrate the utility of the device by isolating CTCs directly from blood samples from patients with metastatic prostate

cancer and conduct molecular profiling of the selected CTCs, which was enabled by the high purity of the selected fractions.

2. Design of the HT-CTC chip

2.1 Design of CTC isolation bed

The design of the HT-CTC chip is presented in Fig. 1(a). It consisted of a CTC isolation bed composed of a parallel array of sinusoidal microchannels with nominal dimensions of 25 μm width, 150 μm depth, and 30 mm length and inlet and outlet channels arrange in a so called Z-configuration. The geometry of the CTC isolation bed is modeled on recent studies by Adams *et al.* and Dharmasiri *et al.,* who have successfully demonstrated use of a network of parallel sinusoidal microfluidic channels decorated with anti-EpCAM monoclonal antibodies (mAbs) for efficiently isolating CTCs directly from blood inputs (Adams et al. 2008; Dharmasiri et al. 2009). The use of the sinusoidal channel geometry provided higher recovery compared to straight channels of the same dimensions. This was attributed to escape of the CTCs' travel from flow streamlines associated with fully developed laminar flow and the Fahraeus-Lindqvist effect (cell focusing to channel centroid), which can be overcome for sinusoidal-shaped channels resulting in a higher probability of cell/wall interactions (Adams et al. 2008). These studies also indicated two other important findings regarding the design of the CTC isolation bed and optimum operating conditions that needed to be considered to achieve maximum cell recoveries. Firstly, at least one dimension of the microchannel must be close to the average diameter of the CTCs (12–25 μm) to promote cell-wall interactions. Secondly, there is an optimal linear flow velocity (2 – 2.5 mm/s) of the CTCs through the microchannels that supports high recoveries. At higher flow velocities, the short residence time of CTC membrane antigens with the surface capture antibodies limits CTC isolation (Adams et al. 2008; Chang and Hammer 1999; Nagrath et al. 2007).

Given these design rules, it was clear that increasing the throughput of the CTC isolation device can be accomplished by increasing the aspect ratio of the sampling channels while keeping their width constant and/or increasing the number of parallel channels in the isolation bed. Fig. 1(b) illustrates an HAR channel with dimensions comparable to a typical CTC but larger than an average WBC. The effect of the number of microchannels comprising the isolation bed and their aspect ratio on the time required to process 7.5 ml of blood through the HT-CTC device at the optimal flow velocity is demonstrated in Fig. 1(c). Clearly, high aspect ratio microchannels offer a practical solution for increasing the throughput. For example, the device originally reported by Adams *et al.* (Adams et al. 2008) used 51 parallel channels (cross-section 30 μm × 150 μm) and would require nearly 4.7 h to process 7.5 ml of blood. By increasing the number of channels to 500 and depth to 250 μm, the same input volume could be processed in <17 min using the same average linear velocity of 2 mm/s. One should also note that high aspect ratio microchannels with aspect ratio equal to AR could not be simply replaced by low aspect ratio microchannels with aspect ratio equal to 1/AR; the beneficial effect of the sinusoidal geometry would be negated.

2.2. Design of inlet and outlet channels – Z-configuration

Previously reported studies have utilized triangular inlet/outlet regions to address the parallel channels in the CTC isolation bed (Fig. 2) (Adams et al. 2008; Dharmasiri et al. 2009). Critical to device efficiency, flow through the capture channels should be uniform, remaining at a linear velocity of 2 mm/s to optimize CTC recovery (Adams et al. 2008; Dharmasiri et al. 2009; Chang and Hammer 1999). Using CFD simulations of a numerically tractable model, where triangular inlet/outlet regions connected 51 sinusoidal channels, we validated that flow is clearly uniformly distributed in the previously reported device, only deviating slightly through the outer channels, where viscous drag along the inlet/outlet walls by the no-slip condition reduced flow velocity (Fig. 2a). Practically, however, the fluid's velocity through the relatively large, triangular regions is slow (roughly 0.2 mm/s) compared to the capture channels, and we have observed that pressure differences within these regions were not great enough to displace air bubbles inadvertently introduced into the system during operation (Fig. 2(b)). The presence of air bubbles can disrupt optimal flow distribution and decrease the efficiency of CTC capture. We have also observed that CTCs as well as contaminating WBCs were occasionally non-specifically trapped around the air-liquid interface at the bubble surface and were difficult to control during subsequent processing steps, such as bed washing and cell staining. For example, CTCs that were not bound to the surface via antigen-antibody interactions could be lost during bed washing at higher flow rates, thus negatively impacting the recovery, whereas some WBCs adhering to the surfaces in the triangular inlet/outlet were not efficiently removed from the device due to lower shear stress observed in these sections, which led to overall lower purity. These aspects were of considerable concern for isolation beds comprised of larger numbers of parallel microchannels.

To alleviate these issues, we adopted herein another fluidic architecture to uniformly address a large array of parallel microchannels within the selection bed, the so called Z-configuration (Figs 1(a) and 2(c)). The Z-configuration is a geometry well known in the field of fuel cells (Zhang et al. 2009). In this configuration, fluid enters the selection bed through a single inlet channel poised perpendicular to an array of microchannels comprising the CTC isolation bed and exits also through a single outlet channel that is also perpendicular to the sinusoidal microchannels. The Z-configuration provides the smallest possible footprint for addressing the isolation bed of the device as only two microchannels are added to the footprint of the selection bed independent of the number of channels being addressed. For example, in a recently proposed fluidic design for neutrophil isolation (Kotz et al. 2010), bifurcation was used for addressing parallel channels of the isolation bed. Using this design, the footprint of the proposed device nearly doubled in order to allocate space for the fluid distribution network.

Because the Z-configuration is a highly parallel system, flow distribution is uniquely sensitive to the length and number of capture channels; thus, a smaller, numerically tractable CFD model as the one used for the triangular inlet/outlet simulations described above is not representative of the Z-configuration shown in Fig. 1(a). To analyze the Z-configuration device, we have employed a mathematical model that segments the system into individual, interconnected fluidic resistors and accurately solves for flow distribution by

conglomerating the pressure and mass balance equations governing flow through each resistor (Zhang et al. 2009). From Fig. 2(a), it is clear that flow in the Z-configuration is also uniformly distributed. Here, the slight parabolic skew occurs by an entirely different phenomenon than viscous drag (Zhang et al. 2009). In this sense, the Z-configuration's primary advantage is that flow through the inlet/outlet channels is typically faster than 2 mm/s, ensuring sufficient pressure to remove any air bubbles introduced during processing (Fig. 2(c)) and optimal flow is maintained throughout the entire analysis process. Furthermore, just as the high aspect ratio capture channels enable faster sample processing, it is possible to further increase volumetric throughput by arraying additional high aspect ratio channels in a Z-configuration without sacrificing device footprint (Kamande et al. 2013).

3. Fabrication and characterization of HT-CTC chips

Application of the HT-CTC devices presented herein for clinical testing required that they are manufactured as disposable units in order to avoid sample carry-over and cross-contamination artifacts during analysis. This requirement required that the chips needed to be produced in high volumes and at low unit costs to be successfully implemented for clinical testing (Chin et al. 2012). Micromanufacturing techniques using polymer substrates fulfill these requirements as polymers are generally inexpensive and a variety of low-cost fabrication techniques are available for both rapid prototyping and mass production of finished devices and with high aspect ratio (Becker and Gartner 2000; Becker and Locascio 2002; Soper et al. 2000). Significant cost advantages as compared to other polymer microfabrication techniques can be realized when using replication techniques such as casting, hot embossing, or injection molding. Among the replication techniques, injection-molding is considered to be the least expensive for mass production of devices. However, it also carries the highest initial capital costs associated with mold master fabrication, machine set-up, and molding condition optimization (Becker and Gartner 2000). For the purpose of the research presented herein, we employed hot embossing as the approach for fabrication of the HT-CTC devices. It is important to realize that microfluidic devices developed using hot embossing can be transferred into production via injection molding with relative ease as the same thermoplastic polymers are used and similar design rules need to be followed during device development. This approach avoids or at least minimizes well recognized problems in the future associated with transferring academic ideas into manufacturable products due to incompatibility of the materials and microfabrication methods between early development and high-volume production (Chin et al. 2012).

The first step in microfabrication of microfluidic devices using hot-embossing is the fabrication of the molding master. Herein, the molding master was fabricated in brass via high-precision micromilling (HPMM) using a commercial milling machine (KERN 44, KERN Micro- und Feinwerktechnik GmbH & Co.KG; Murnau, Germany) and solid carbide tools (500 μm, 200 μm, and 100 μm diameter (Performance Micro Tool, Janesville, WI)) using procedures previously described in detail (Hupert et al. 2007). Briefly, the surface of a 6.3 mm thick, 120 mm diameter circular brass plate (alloy 353 engravers brass, McMaster-Carr, Atlanta, GA) was pre-cut with a 500 μm diameter milling bit to ensure parallelism between both faces of the brass plate and uniform height of the final milled microstructures

over the entire pattern. This was followed by a rough milling of the microstructures using a 500 μm and 200 μm milling bits, and a finishing cut with either 200 μm or 100 μm diameter milling bit depending on the smallest distance between milled structures. Micromilling was carried at 50,000 rpm at feed rates that were dependent on the size of the milling bit and were typically in the range of 200 mm/min for a 500 μm bit, 100 – 150 mm/min for 200 μm bit, 50 – 75 mm/min for 100 μm bit.

HPMM offers significant advantages over other mold master fabrication methods such as X-ray-LiGA or UV-LiGA as it allows for shorter turnaround times, low cost, and single step fabrication of multi-level structures (Becker and Locascio 2002; Soper et al. 2000; Hupert et al. 2007). Although HPMM is not capable of achieving the fine resolution or minimum feature size of lithography-based techniques (*i.e.,* sub-μm for X-ray LiGA) due to milling bit size limitations, it is well suited for many microfluidic applications, which usually require structures in the range of 10 – 500 μm with aspect ratios (<20) and inter-structure spacing (>30 μm) easily obtainable using micromilling, such as that required for the CTC selection device shown in Fig. 1 and 2. Fig. 3(a) presents the brass mold master used for replication of the HT-CTC beds with 50, 100, and 150 sinusoidal channels. Fig. 3(b) presents an example of multilevel structures used to replicate receiving ports (Fig. 3(c)) required for mounting capillary tubing for minimal stress applied to the blood sample during introduction into the microfluidic network. Fig. 3(d) presents a picture of assembled HT-CTC devices, which could be scaled from 50 to 320 microchannels depending on the blood volume processing needs while keeping the processing time below 45 min irrespective of the input volume.

HT-CTC chips were replicated into cyclic olefin copolymer (Topas 6013)S-04, Topas Advanced Polymers, Florence KY) using hot embossing (HEX-03, Jenoptik Optical Systems GmbH, Jena, Germany) at the following conditions: embossing temperature 155°C, embossing force 30 kN, embossing time 120 s, de-molding temperature 122 °C. Fig. 4 presents SEM images of hot embossed HT-CTC beds. Clearly, high quality replication of the HAR microchannels (AR = 6) was achieved. The average dimensions for the sinusoidal microchannels were as follows: width measured at the bottom of the microchannel (WB) was 20.0 ± 1.0 μm; width measured at the top (WT) was 27.4 ± 0.8 μm and microchannel depth was (D) was 152.0 ± 1.0 μm. The dimensions indicate a trapezoidal shape of the channel cross-section with slightly tapered walls with an average draft angle of 1.4°. This draft angle was not intentionally imposed by the mold fabrication because straight (not tapered) milling bits were used during molding master fabrication. It was rather the result of selected milling conditions and flexing of the micromilling tools during brass removal. Draft angles of this magnitude are very advantageous for the replication process as they reduce friction between the molded part and mold master during de-molding, thus reducing replication errors due to polymer pull-out and prolonging the molding master usable lifetime.

SEM investigation of the sidewalls of the microchannels also revealed the presence of the characteristic side wall roughness, which was a direct result of using a micromilled brass molding master for hot embossing (inset in Fig. 4(b)). This roughness was caused by transfer of the milling marks left on the sidewalls of the brass microstructures from the milling process by the imperfections of the cutting edge of the milling bit (Hupert et al.

2007). The milling marks propagate in the same direction as the milling bit movement (parallel to the molding master floor) and lead to different sidewall roughness measured in a horizontal direction versus one measured vertically. The typical values for sidewall roughness were 55 nm average roughness (R_a) and 200 nm mean peak height (R_{pm}) when measured horizontally along the channel wall, and 115 nm and 290 nm for R_a and R_{pm}, respectively, when measured vertically (Hupert et al. 2007). For comparison, the typical R_a of the polymer material used as the stock for hot embossing was less than 20 nm.

It has been reported that sidewall roughness larger than 80 nm RMS (or ~73 nm R_a) is detrimental to the quality of the hot embossed structures and long term stability of molding masters for micro-replication of the structures with aspect ratios above 0.5 (Becker and Heim 2000) for highly vertical sidewalls such as those produced with the LiGA process (Yuhua et al. 2007). Interestingly, the sidewall roughness of this magnitude observed in our studies had no noticeable effect on the replication fidelity of the HAR channels (AR = 6) and mechanical and dimensional stability of the molding master over prolonged use, which is probably due to the beneficial effect of the 1.4° taper observed for microstructures produced via HPMM. To date, we were able to successfully perform over 500 replication cycles using a single brass mold master without a noticeable reduction of the quality of the embossed structures or deterioration of the master. For example, the average microchannel dimension measured after the first 30 embossing cycles were 20.0 ±1 μm × 27.4 ±0.8 μm × 152 ±1 μm (WB × WT × D), whereas the corresponding dimensions for the microchannels measured after 300 embossing cycles were 19.7 ± 0.5 μm × 27.8 ± 1.0 μm × 152 ±1 μm. Clearly, measured dimensions of the HAR microchannels are well within the measurement error indicating high dimensional stability of the molding master and long term reproducibility of the hot embossing process.

Following hot embossing, the next step in device fabrication is enclosing the fluidic network with a cover plate made from the same material as the substrate, in this case COC. The process we employed herein is thermal fusion bonding in which the cover plate and substrate, following UV activation (see below) are brought into conformal contact under a fixed pressure and then slowly heated to a temperature slightly below the T_g of the thermoplastic. Specifically, we used a temperature of 132°C and a bonding pressure of ~1 N/cm^2. Bonding conditions were carefully selected to achieve high bond strength, but preserve as much as possible structural integrity of the HAR microchannels. Comparison of Fig. 4(c) and Fig. 4(d) shows that slight deformation of the HAR microchannel was observed during the thermal fusion bonding process as noted in the inset of Fig. 4(d).

4. Modification of High Aspect Ratio, Polymeric Microstructures for the Immobilization of Antibodies

Critical to the positive selection of CTCs in our devices and many bioassays in general, recognition elements must be appropriately attached, preferably via covalent interactions, to surfaces within the HAR sinusoidal microchannels. While several avenues for such attachments are possible, the method most compatible with mass producible polymer devices is the irradiation of selection surfaces with UV light to generate carboxylic acid groups that are reactive to amine-bearing biologics, such as monoclonal antibodies. This UV

activation modality has been studied extensively for a number of thermoplastics (McCarley et al. 2005), but only recently has the UV activation of high aspect ratio, polymer microchannels been investigated (Jackson et al. 2013). To activate the HAR microchannel surfaces, the majority of the UV radiation's flux must first pass through the bulk material. Thus, the optimal transmissivity of the polymeric substrate is critical, especially as the microchannel's aspect ratio increases (Jackson et al. 2013).

We studied this effect for two polymers, PMMA and COC. Transmissivity of PMMA measured at 254 nm (T_{254nm}) has shown poor characteristics as it has changed from 1.2 to 0.5 % over the course of a 15 min UV activation time using a low pressure, broadband Hg lamp with power density of 22 mW/cm^2 measured at 254 nm. On the other hand, COC has shown excellent optical properties as the $T_{254\ nm}$ changed from 53.8 to 36.8 % during the same course of UV treatment. Next, within UV-activated and thermal fusion bonded microchannels, we reacted fluorescently labeled Cy3-oligonucleotides with surface-confined carboxylic acids via a 5'-pendant amino group on the oligonucleotide, thereby measuring activation efficiency via fluorescence intensity. The fluorescence signal within COC microchannels was 4.68 ±0.80 times greater than PMMA microchannels as acquired through the assembled microdevices' cover plate (Fig. 5). We then exposed the microchannel sidewalls by cutting along their lengths with a band saw and observed an intriguing effect of the bulk polymer's absorption of UV radiation (Fig. 6). An activation gradient was observed along the depth of the PMMA sidewalls, decreasing from 384 ±81 cps in the top third of the channel to nearly background fluorescence below (112 ±55 cps). In the case of the COC microchannel, the degree of activation as noted by the fluorescence intensity was significantly greater and more uniform throughout its depth (2233 ±310 cps). The impact of these observations culminated in an increase in both the recovery and purity of CTC capture using CTC isolation units fabricated in COC polymer as opposed to PMMA (Jackson et al. 2013). Based on these findings, we selected COC as the primary material for fabrication of the HT-CTC chips. All clinical studies reported below were performed using this material.

5. Isolation of CTCs from cancer patients

As a demonstration of the utility of the HT-CTC device for isolating CTCs from blood, we processed blood samples spiked with cultured MCF7 cells and blood samples secured from patients with metastatic prostate cancer. First, the surface of the microfluidic channels of UV activated and assembled COC HT-CTC devices was modified using well established EDC-NHS chemistry (20 mg/ml EDC, 2 mg/ml NHS, in 100 mM MES, pH 5.2) followed by the incubation with a solution of anti-EpCAM monoclonal antibody (0.5 mg/ml; 150 mM PBS buffer, pH 7.4) overnight at 4°C (Adams et al. 2008). This activation protocol produced the surfaces of microchannel with covalently bound anti-EpCAM antibodies in near monolayer coverage, which is required for selective affinity-based isolation of CTC expressing EpCAM antigens. Blood was processed through the device using a volumetric flow rate of 23 μL/min required to achieve a 2 mm/s average sample flow velocity in the sinusoidal microchannels. After isolation and washing, captured cells were fixed (2–4% paraformaldehyde), permeabilized (0.1% Triton X-100), and stained using a standard panel of fluorescently labeled markers commonly used for CTC analysis including epithelial markers (Texas Red-labeled anti-Cytokeratins 7/8/pan), nucleus stain (DAPI), and a negative control consisting

of FITC labeled leukocyte antibody CD45; the stained cells were characterized using fluorescence microscopy.

Fig. 7(a) presents fluorescence images of MCF7 cells captured within the sinusoidal channels of the isolation bed. Two prostate cancer CTCs are shown in Fig.7(b) and display the necessary characteristics of CTCs, including positive staining for DAPI (blue) and Cytokeratins (red), and lack of staining for CD45 (green) (Nagrath et al. 2007). Also the large nucleus to cytoplasm ratio observed for these cells is distinctive for CTCs. Fig. 7(c) shows a summary of the number of CTCs and contaminating WBCs isolated from blood samples from 9 patients with prostate cancer who donated their blood under a protocol approved by the University of North Carolina Institutional Review Board. The number of CTC detected per 1 ml of blood ranged from 19 to 76 (average = 39 ±19) whereas the number of contaminating WBCs was much lower and relatively stable between all analyzed samples (range 2 to 8, average = 6 ±2). These data indicate very high purity of isolated CTCs with the average purity expressed as the ratio between number of CTCs and the total number of CTCs and WBCs (purity = 86 ± 6%). We believe that such high purity was a direct result of well controlled, high shear forces acting on the non-specifically bound WBCs during the bed washing step.

Given such high purity of the selection process, we attempted to molecular profile the isolated CTCs. For this, 2.5 ml of patient blood was processed through the anti-EpCAM modified HT-CTC chip, washed with PBS buffer, and the total RNA from the cells captured was extracted and purified using a commercial RNeasy micro kit (Qiagen) with a slightly modified protocol. The reverse transcription was performed using SuperScript III reverse transcriptase (Invitrogen) and an aliquot of purified RNA. Finally, the resulting cDNA underwent a PCR using 6 sets of primers targeting GAPDH (housekeeping gene control), PSMA (prostate-specific membrane antigen), PSA (prostate-specific antigen), CK19, androgen receptor, and EpCAM. As expected, PSMA, PSA, androgen receptor, and EpCAM show strong bands while there was no band for the CK19 gene indicating that successful molecular profiling can be achieved on the population of CTCs isolated directly from the patient blood using the HT-CTC device.

6. Conclusions

We have developed and tested disposable, all-polymer, microfluidic device for efficient, high-throughput isolation of CTCs directly from blood. The device employed isolation bed consisting of an array of HAR, parallel, sinusoidal microchannels with walls covalently decorated with anti-EpCAM antibodies to provide selective, affinity-based capture of CTCs. We have successfully adopted Z-configuration of inlet and outlet channels to uniformly address CTC isolation bed and eliminate presence of persistent air bubbles that may affect analytical performance of the device. We have also evaluated PMMA and COC as substrate materials for construction of HT-CTC devices and shown that COC possesses superior optical properties for efficient UV activation of HAR microfluidic channels, which result in higher density and more uniform coverage of the microchannel surface with antibodies. Finally, we have tested the device utility by isolating CTCs directly from blood from patients with metastatic prostate cancer, and molecular profiling of isolated CTCs.

Acknowledgments

The authors would like to thank the NIH (R01-EB010087; N43CO-2010-00066 (NCI-SBIR)), the University of North Carolina (UNC), the University Cancer Research Fund (UNC) and the World Class University Program in Korea for financial support of this work. The authors would also like to thank the UNC Olympus Imaging Research Center for providing the use of the microscope for CTC imaging, UNC-Chapel Hill Analytical and Nanofabrication Laboratory (UNC-CHANL) for access to hot embossing machine and SEM facilities, and North Carolina State University Precision Instrument Machine Shop for fabrication of molding masters.

References

Adams AA, Okagbare PI, Feng J, Hupert ML, Patterson D, Goettert J, McCarley RL, Nikitopoulos D, Murphy MC, Soper SA. Highly efficient circulating tumor cell isolation from whole blood and label-free enumeration using polymer-based microfluidics with an integrated conductivity sensor. J Am Chem Soc. 2008; 130(27):8633–8641. [PubMed: 18557614]

Allard WJ, Matera J, Miller MC, Repollet M, Connelly MC, Rao C, Tibbe AG, Uhr JW, Terstappen LW. Tumor cells circulate in the peripheral blood of all major carcinomas but not in healthy subjects or patients with nonmalignant diseases. Clin Cancer Res. 2004; 10(20):6897–6904. [PubMed: 15501967]

Becker H, Gartner C. Polymer microfabrication methods for microfluidic analytical applications. Electrophoresis. 2000; 21(1):12–26. [PubMed: 10634467]

Becker H, Heim U. Hot embossing as a method for the fabrication of polymer high aspect ratio structures. Sensor Actuat A: Phys. 2000; 83(1–3):130–135.

Becker H, Locascio LE. Polymer microfluidic devices. Talanta. 2002; 56(2):267–287. [PubMed: 18968500]

Chang KC, Hammer DA. The forward rate of binding of surface-tethered reactants: effect of relative motion between two surfaces. Biophys J. 1999; 76(3):1280–1292. [PubMed: 10049312]

Chin CD, Linder V, Sia SK. Commercialization of microfluidic point-of-care diagnostic devices. Lab Chip. 2012; 12(12):2118–2134. [PubMed: 22344520]

Dharmasiri U, Balamurugan S, Adams AA, Okagbare PI, Obubuafo A, Soper SA. Highly efficient capture and enumeration of low abundance prostate cancer cells using prostate-specific membrane antigen aptamers immobilized to a polymeric microfluidic device. Electrophoresis. 2009; 30:1–12. [PubMed: 19156666]

Dharmasiri U, Njoroge SK, Witek MA, Adebiyi MG, Kamande JW, Hupert ML, Barany F, Soper SA. High-Throughput Selection, Enumeration, Electrokinetic Manipulation, and Molecular Profiling of Low-Abundance Circulating Tumor Cells Using a Microfluidic System. Anal Chem. 2011; 83(6): 2301–2309. [PubMed: 21319808]

Dharmasiri, U.; Witek, MA.; Adams, AA.; Soper, SA. Microsystems for the Capture of Low-Abundance Cells. In: Yeung, ES.; Zare, RN., editors. Ann Rev Anal Chem, vol 3. Annual Review of Analytical Chemistry. 2010. p. 409-431.

Farace F, Massard C, Vimond N, Drusch F, Jacques N, Billiot F, Laplanche A, Chauchereau A, Lacroix L, Planchard D, Le Moulec S, Andre F, Fizazi K, Soria JC, Vielh P. A direct comparison of CellSearch and ISET for circulating tumour-cell detection in patients with metastatic carcinomas. Brit J Cancer. 2011; 105(6):847–853. [PubMed: 21829190]

Hou J, Krebs MG, Ward T, Morris K, Sloane R, Blackhall FH, Dive C. Circulating Tumor Cells, Enumeration and Beyond. Cancers. 2010; 2(2):1236–1250. [PubMed: 24281115]

Hupert ML, Guy WJ, Llopis SD, Shadpour H, Rani S, Nikitopoulos DE, Soper SA. Evaluation of micromilled metal mold masters for the replication of microchip electrophoresis devices. Microfluid Nanofluid. 2007; 3(1):1–11.

Jackson JM, Witek MA, Hupert M, Brady C, Pullagurla S, Kamande J, Aufforth R, Tignanelli CJ, Torphy RJ, Yeh JJ, Soper SA. UV activation of polymeric high aspect ratio microstructures: ramifications in antibody surface loading for circulating tumor cell selection. Lab Chip [Online early access]. 2014

Kamande JW, Hupert ML, Witek MA, Wang H, Trophy R, Dharmasiri U, Njoroge SK, Jackson JM, Aufforth R, Snavely A, Yeh JJ, Soper SA. Modular microsystem for the isolation, enumeration,

and phenotyping of circulating tumor cells: managing patients with pancreatic cancer. Anal Chem [Online early access]. 2013

Kotz KT, Xiao W, Miller-Graziano C, Qian W-J, Russom A, Warner EA, Moldawer LL, De A, Bankey PE, Petritis BO, Camp DG, Rosenbach AE, Goverman J, Fagan SP, Brownstein BH, Irimia D, Xu W, Wilhelmy J, Mindrinos MN, Smith RD, Davis RW, Tompkins RG, Toner M. Clinical microfluidics for neutrophil genomics and proteomics. Nat Med. 2010; 16(9):1042–1047. [PubMed: 20802500]

Kuo JS, Zhao Y, Schiro PG, Ng L, Lim DSW, Shelby JP, Chiu DT. Deformability considerations in filtraction of biological cells. Lab Chip. 2010; 10:837–842. [PubMed: 20379567]

Lin YG, Merritt WM, Spannuth WA, Nick AM, Stone RL, Tsinberg P, Coleman RL, Birrer MJ, Bischoff F, Sood AK. Rare circulating tumor cells can be reliably and efficiently detected using a novel microfluidics and micro-electromechanical systems (MEMS)-based rare cell recovery platform: Preclinical and clinical data. Gynecol Oncol. 2009; 112(2):230.

Maheswaran S, Haber DA. Circulating tumor cells: a window into cancer biology and metastasis. Curr Opin Genet Dev. 2010; 20(1):96–99. [PubMed: 20071161]

Maheswaran S, Sequist LV, Nagrath S, Ulkus L, Brannigan B, Collura CV, Inserra E, Diederichs S, Lafrate AJ, Bell DW, Digumarthy S, Muzikansky A, Irimia D, Settleman J, Tompkins RG, Lynch TJ, Toner M, Haber DA. Detection of Mutations in EGFR in Circulating Lung-Cancer Cells. New Engl J Med. 2008; 359:366–377. [PubMed: 18596266]

McCarley RL, Vaidya B, Wei S, Smith AF, Patel AB, Feng J, Murphy MC, Soper SA. Resist-Free Patterning of Surface Architectures in Polymer-Based Microanalytical Devices. J Am Chem Soc 127 (Copyright (C) 2012 American Chemical Society (ACS). All Rights Reserved. 2005:842–843.

Mostert B, Kraan J, de Vries JB, van der Spoel P, Sieuwerts AM, Schutte M, Timmermans AM, Foekens R, Martens JWM, Gratama J-W, Foekens JA, Sleijfer S. Detection of circulating tumor cells in breast cancer may improve through enrichment with CD-146. Breast Cancer Res Tr. 2011; 127:33–41.

Nagrath S, Sequist LV, Maheswaran S, Bell DW, Irimia D, Ulkus L, Smith MR, Kwak EL, Digumarthy S, Muzikansky A, Ryan P, Balis UJ, Tompkins RG, Haber DA, Toner M. Isolation of rare circulating tumour cells in cancer patients by microchip technology. Nature (London, U K). 2007; 450(7173):1235–1239. [PubMed: 18097410]

Nakagawa T, Martinez SR, Goto Y, Koyanagi K, Kitago M, Shingai T, Elashoff DA, Ye X, Singer FR, Giuliano AE, Hoon DS. Detection of circulating tumor cells in early-stage breast cancer metastasis to axillary lymph nodes. Clin Cancer Res. 2007; 13(14):4105–4110. [PubMed: 17634536]

Saliba A-E, Saias L, Psychari E, Minc N, Simon D, Bidard F-C, Mathiot C, Pierga J-Y, Fraisier V, Salamero J, Saada V, Farace F, Vielh P, Malaquin L, Viovy J-L. Microfluidic sorting and multimodal typing of cancer cells in self-assembled magnetic arrays. P Natl Acad Sci. 2010; 107(3)):14524–14529.

Sieuwerts AM, Kraan J, Bolt J, van der Spoel P, Elstrodt F, Schutte M, Martens JWM, Gratama JW, Sleijfer S, Foekens JA. Anti-epithelial cell adhesion molecule antibodies and the detection of circulating normal-like breast tumor cells. J Nat Cancer I. 2009; 101:61–66.

Smirnov DA, Zweitzig DR, Foulk BW, Miller MC, Doyle GV, Pienta KJ, Meropol NJ, Weiner LM, Cohen SJ, Moreno JG, Connelly MC, Terstappen LW, O'Hara SM. Global gene expression profiling of circulating tumor cells. Cancer Res. 2005; 65(12):4993–4997. [PubMed: 15958538]

Soper SA, Ford SM, Qi S, McCarley RL, Kelly K, Murphy MC. Polymeric microelectromechanical systems. Anal Chem. 2000; 72(19):643A–651A.

Stott SL, Lee RJ, Nagrath S, Yu M, Miyamoto DT, Ulkus L, Inserra EJ, Ulman M, Springer S, Nakamura Z, Moore AL, Tsukrov DI, Kempner ME, Dahl DM, Wu C-L, Iafrate AJ, Smith MR, Tompkins RG, Sequist LV, Toner M, Haber DA, Maheswaran S. Isolation and characterization of circulating tumor cells from patients with localized and metastatic prostate cancer. Sci Transl Med. 2010; 2(25):25ra23.

Tan SJ, Yobas L, Lee GYH, Ong CN, Lim CT. Microdevice for the isolation and enumeration of cancer cells from blood. Biomed Microdev. 2009; 11(4):883–892.

Wang S, Liu K, Liu J, Yu ZTF, Xu X, Zhao L, Lee T, Lee EK, Reiss J, Lee Y-K, Chung LWK, Huang J, Rettig M, Seligson D, Duraiswamy KN, Shen CKF, Tseng H-R. Highly Efficient Capture of

Circulating Tumor Cells by Using Nanostructured Silicon Substrates with Integrated Chaotic Micromixers. Angew Chem Int Edit. 2011; 50(13):3084–3088.

Williams, A.; Balic, M.; Datar, R.; Cote, R. Size-Based Enrichment Technologies for CTC Detection and Characterization. In: Ignatiadis, M.; Sotiriou, C.; Pantel, K., editors. Minimal Residual Disease and Circulating Tumor Cells in Breast Cancer, vol 195. Rec Res Cancer. Springer Berlin Heidelberg; 2012. p. 87-95.

Xu Y, Phillips JA, Yan JL, Li QG, Fan ZH, Tan WH. Aptamer-Based Microfluidic Device for Enrichment, Sorting, and Detection of Multiple Cancer Cells. Anal Chem. 2009; 81(17):7436–7442. [PubMed: 19715365]

Yang L, Lang JC, Balasubramanian P, Jatana KR, Schuller D, Agrawal A, Zborowski M, Chalmers JJ. Optimization of an enrichment process for circulating tumor cells from the blood of head and neck cancer patients through depletion of normal cells. Biotechnol Bioeng. 2009; 102(2):521–534. [PubMed: 18726961]

Yuhua G, Liu G, Xiong Y, Jun W, Xinlong H, Tian Y. Study of Hot Embossing Using Nickel and Ni-PTFE LiGA Mold Inserts. J Microelectromech Syst. 2007; 16(3):589–597.

Zhang W, Hu P, Lai X, Peng L. Analysis and optimization of flow distribution in parallel-channel configurations for proton exchange membrane fuel cells. J Power Sources. 2009; 194(2):931–940.

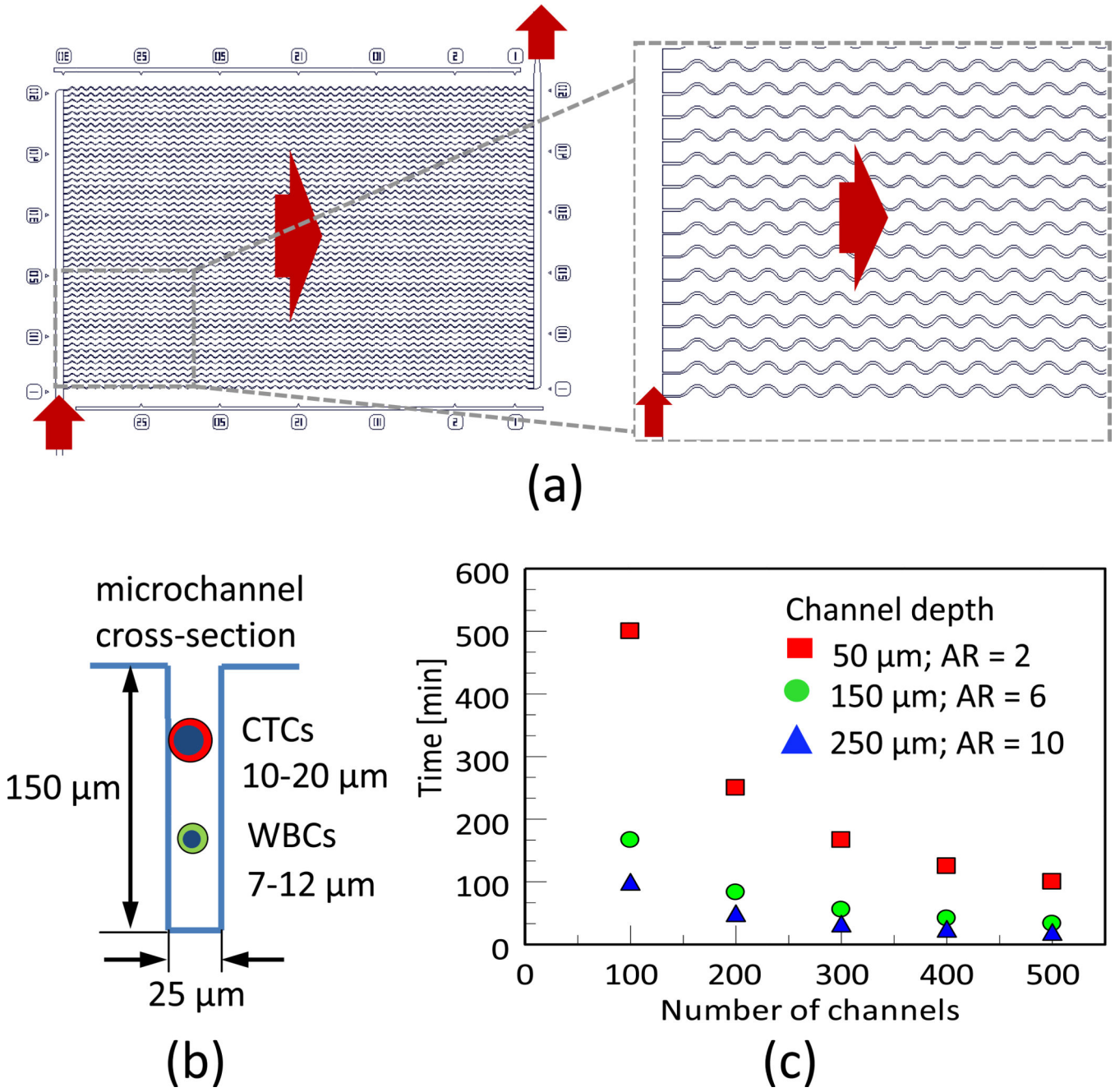

Fig. 1.

(**a**) Schematic representation of the design and operation of the HT-CTC selection chips arranged in a Zconfiguration. (**b**) Diagram of size comparison between microfluidic channel dimensions and the size of a typical CTC and WBC. (**c**) Processing time for 7.5 ml of blood as a function of the microchannel depth and channel number for a channel width of 25 µm and linear flow velocity of 2 mm/s.

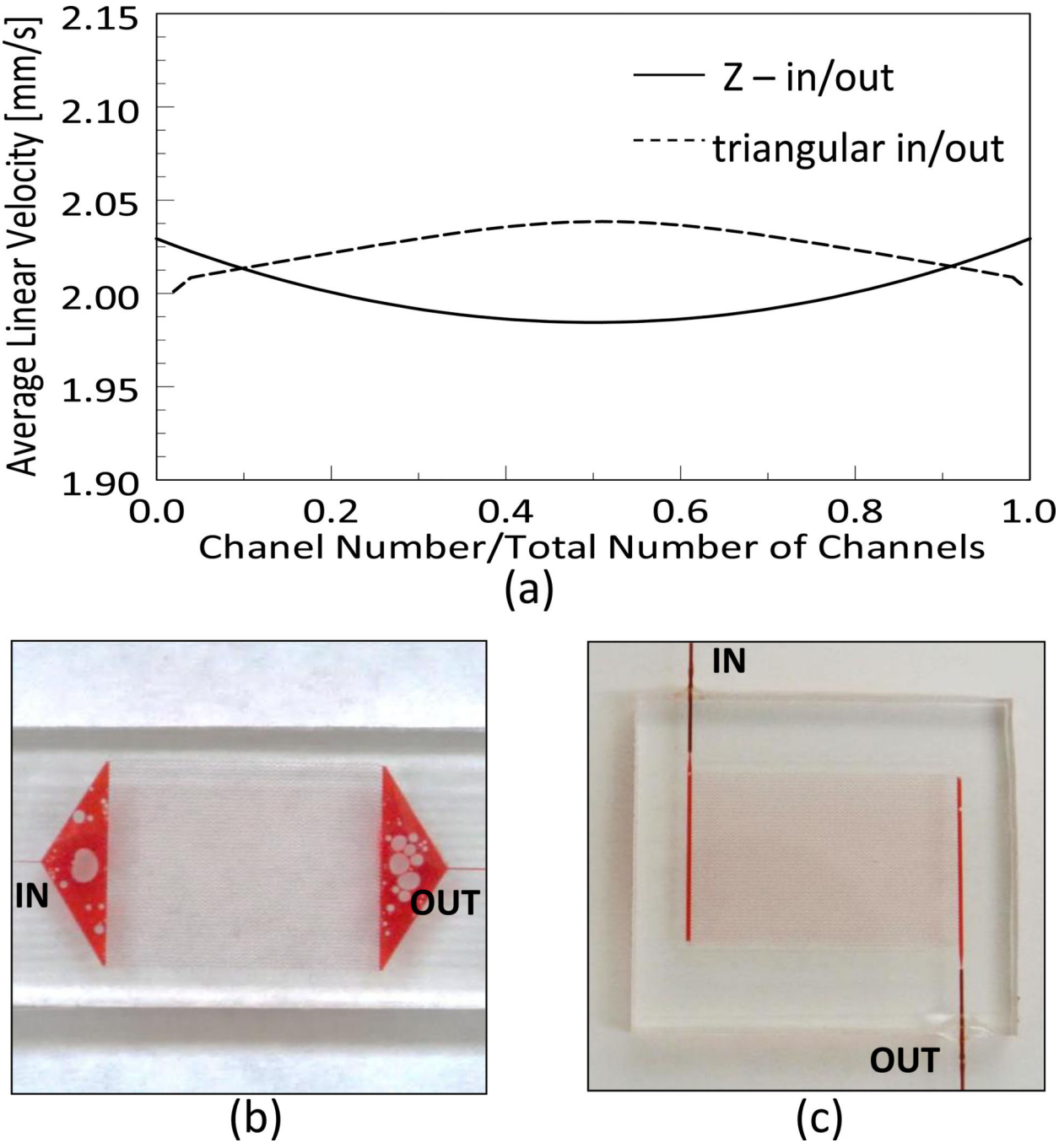

Fig. 2.

Comparison between different inlet/outlet geometries for a CTC microfluidic chip. (**a**) Results of computer simulations for the distribution of flow velocities within the CTC isolation bed with 50 microchannels arranged in a Z-configuration or 51 microchannels with triangular inlets and outlets. Pictures of CTC capture beds filled with blood for the triangular configuration (**b**) and the Z-configuration (**c**).

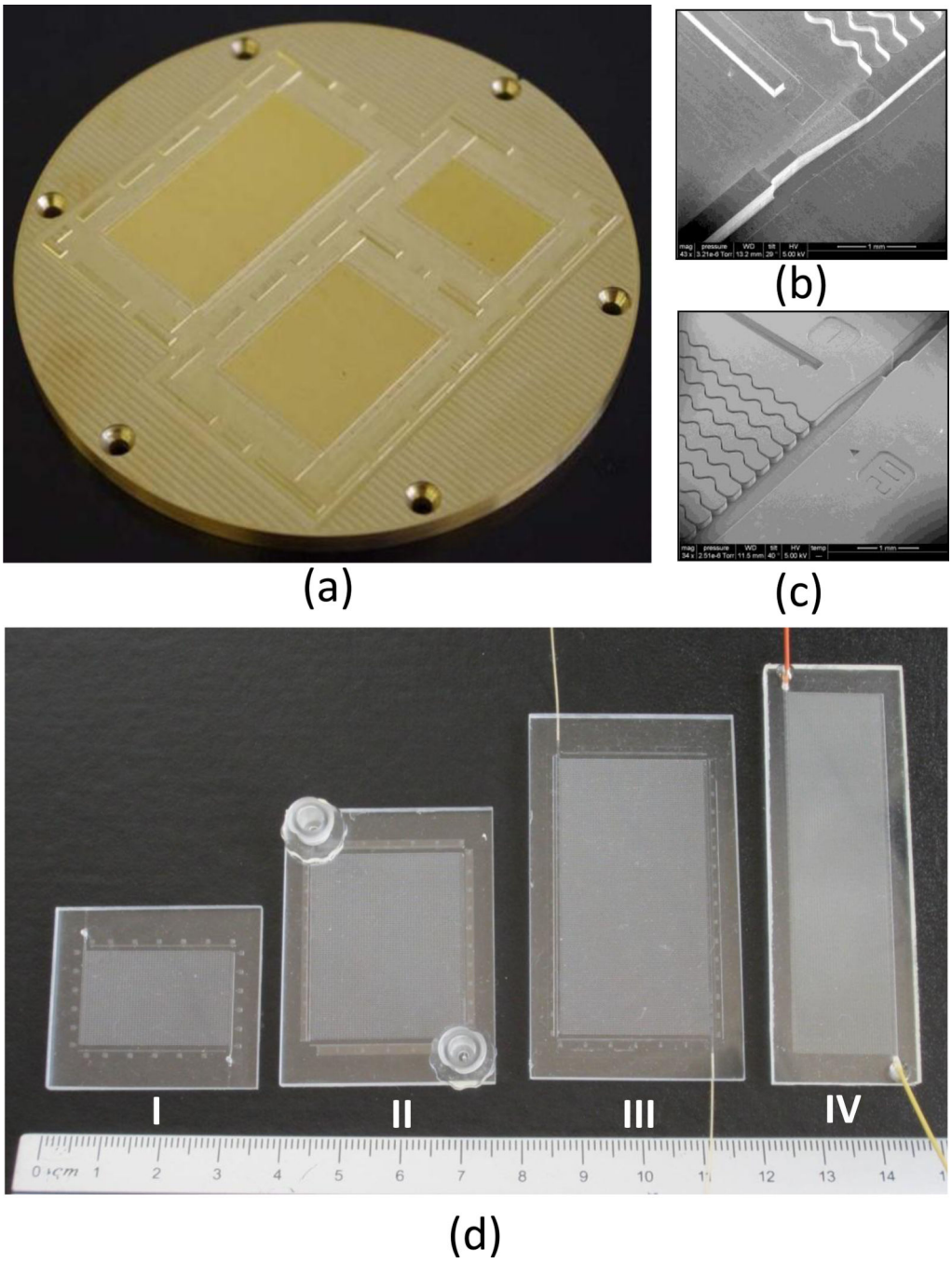

Fig. 3.

(**a**) Picture of a high-precision micromilled brass mold master (120 mm diameter) for hot-embossing HT-CTC chips with 50, 100, and 150 sinusoidal microchannels (microchannel nominal dimensions were 25 μm × 150 μm × 30 mm (WxDxL) and microchannel spacing was 330 μm center-to-center. (**b** and **c**) SEM of a section of the mold master and hot embossed COC HT-CTC selection chip. (**d**) Assembled HT-CTC chips with different numbers of microfluidic channels designed for efficient processing of different sample volumes. (I-III) show chips fabricated using mold insert shown in (**a**); IV – shows a CTC

chip with reduced microchannel spacing (200 um center to center) and single microchannel length of 20 mm which allowed to fit 320 sinusoidal channels within a footprint of a standard microscope slide (25 mm × 75 mm). Various interconnection strategies for sample introduction are also shown.

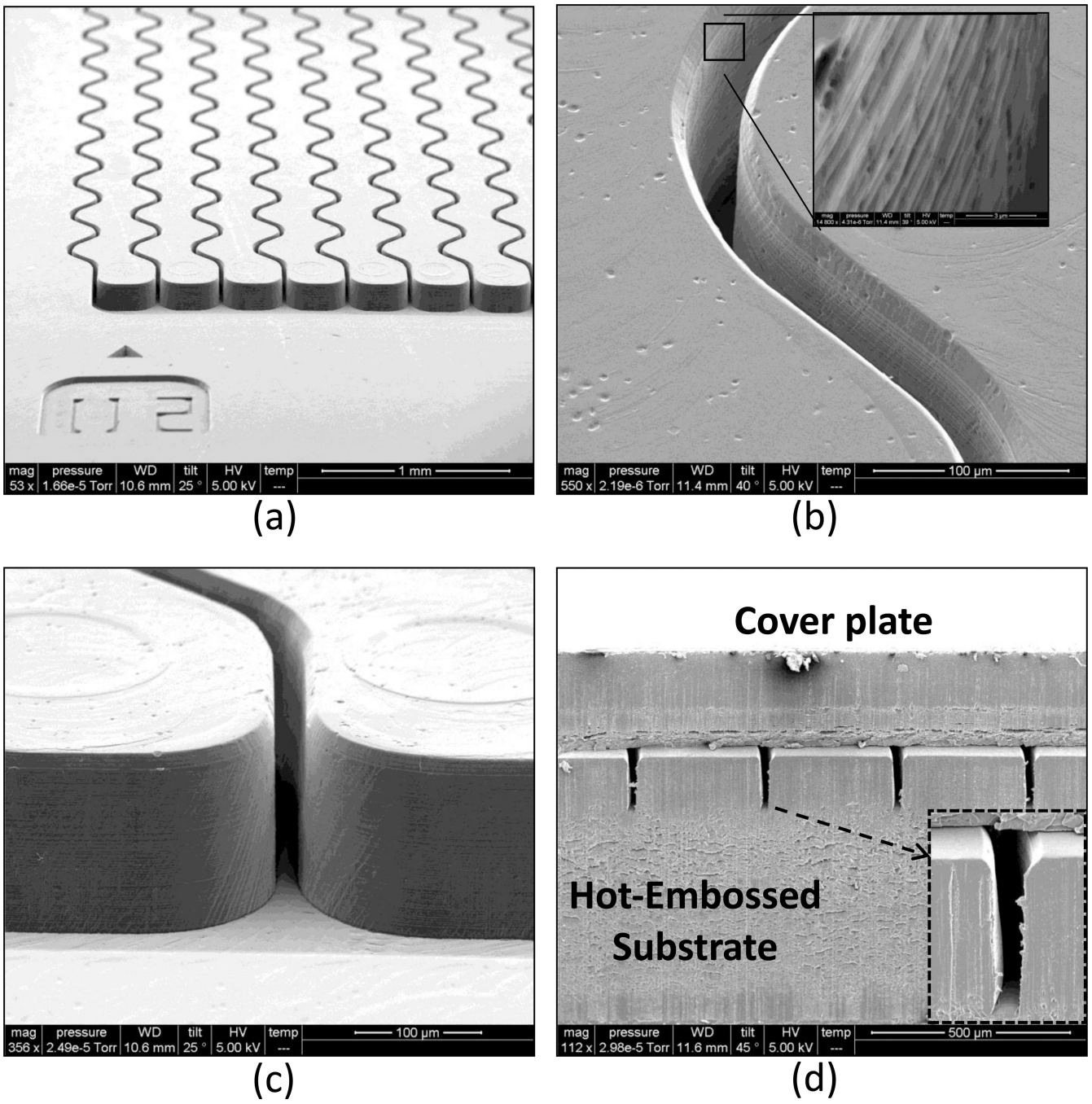

Fig. 4.

SEMs of the HT-CTC chips hot embossed into the thermoplastic, COC. (**a**) Low resolution SEM showing a series of sinusoidal HAR channels. (**b**) High resolution SEM image of one sinusoidal channel with the inset showing surface roughness due to milling. (**c**) SEM of the HAR sinusoidal channel prior to thermal fusion bonding of the cover plate. (**d**) SEM of a HAR channel following thermal fusion bonding of hot embossed HT-CTC chip with the COC cover plate and dicing to reveal microchannel cross-section. Burrs visible on the right side of the microchannel wall (inset) resulted from the dicing process.

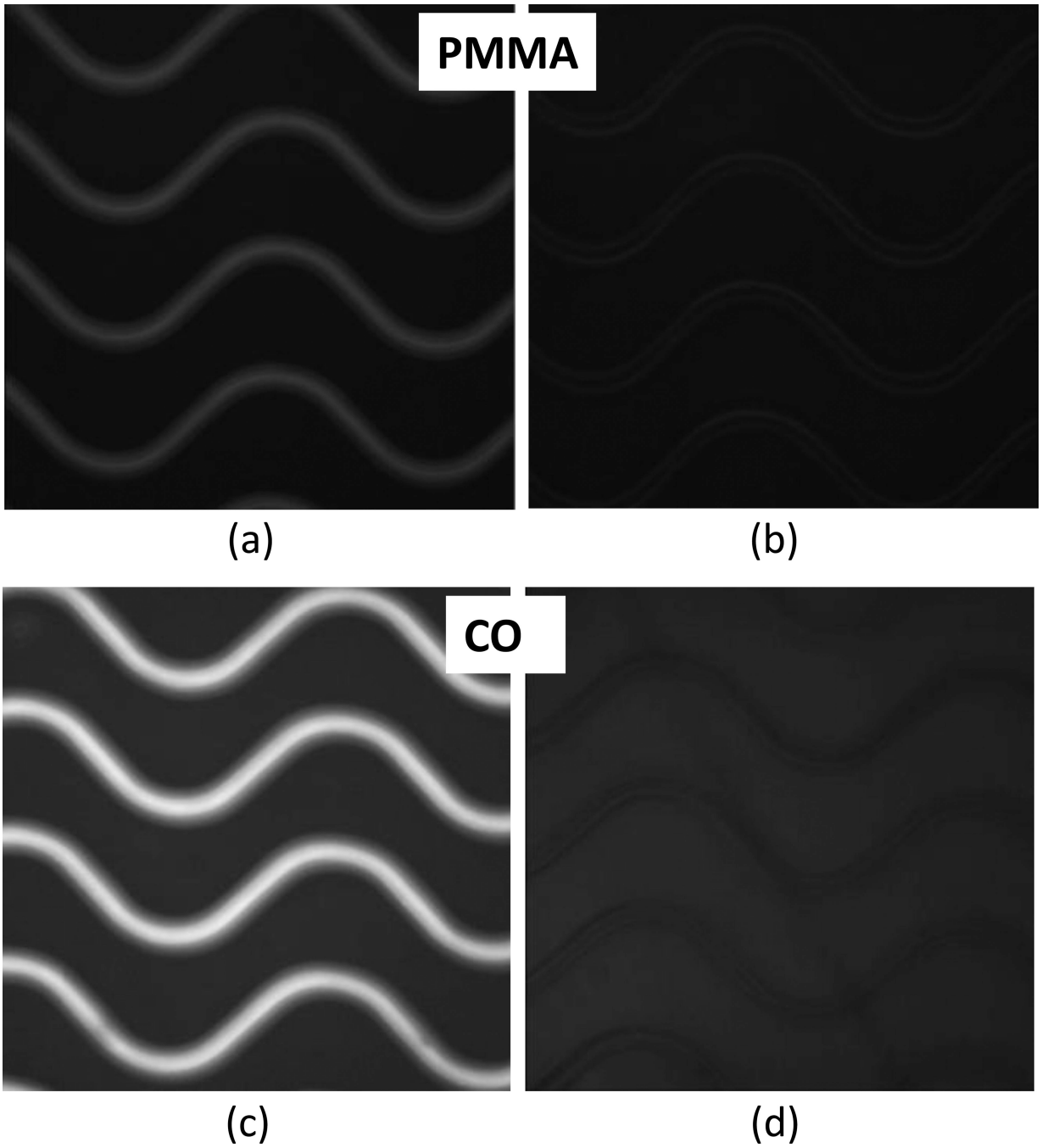

Fig. 5.

Fluorescence imaging of the (**a**) PMMA and (**c**) COC HAR microchannels after UV activation and chemical attachment of dye-labeled oligonucleotides (20 mg/mL EDC, 40 μM oligo-Cy3, pH 7.4, 3 h, RT). Fluorescent intensity of immobilized oligonucleotides indicate activation efficiency within high aspect ratio microstructures. (**b**) PMMA and (**d**) COC contr ols (oligonucleotides introduced without EDC coupling agent) show low nonspecific adsorption and autofluorescence.

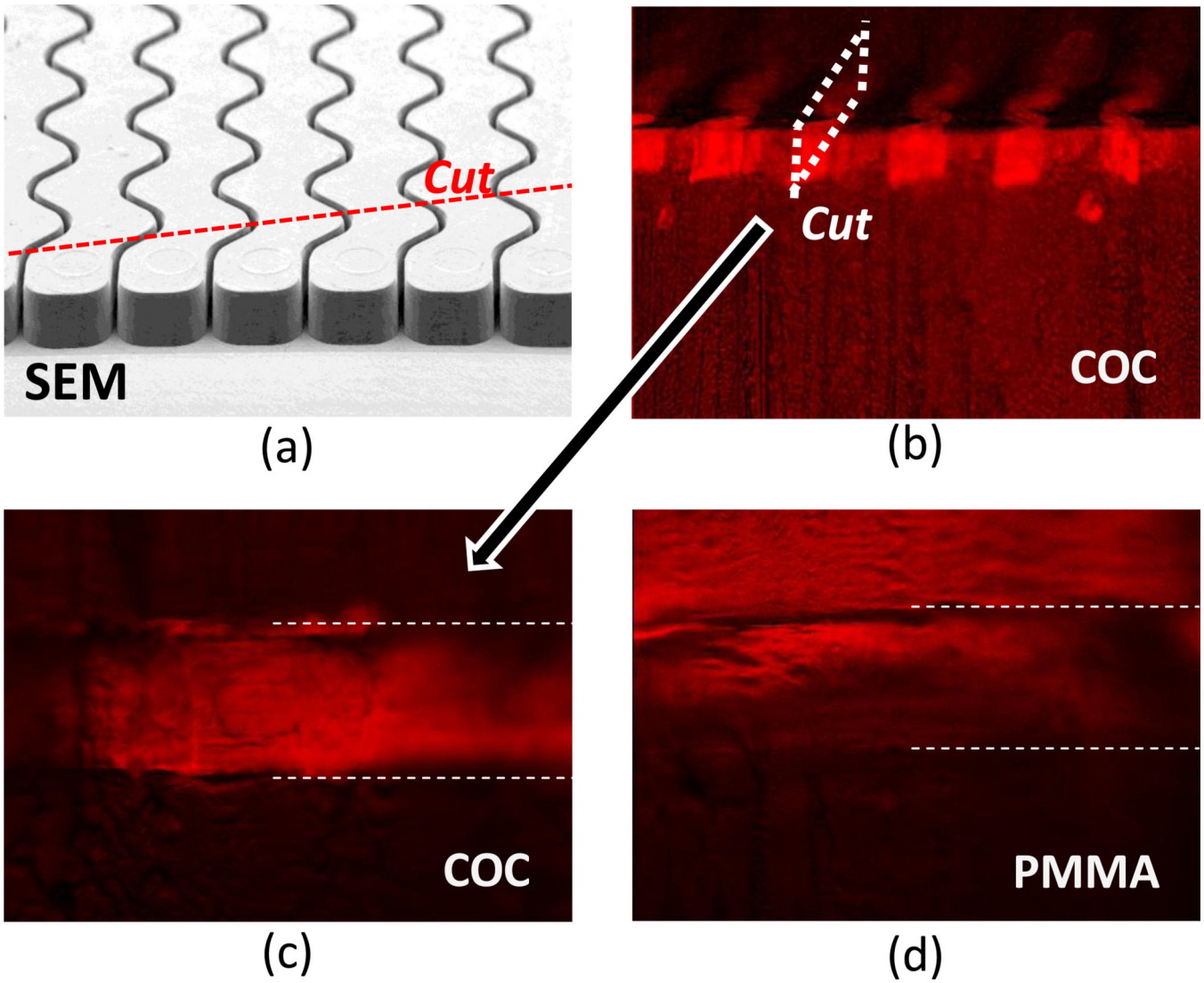

Fig. 6.

Uniformity of the COC and PMMA HAR microchannel modification. (**a**) Schematic representation of how the modified chip was cut to reveal cross-section for fluorescent measurement shown in (**b**). (**b**) Fluorescence imaging of the COC HAR microchannels after UV activation and chemical attachment of dye-labeled oligonucleotides (conditions as in Fig. 5) and schematic representation of cut to reveal side view of the modified channel shown in (**c**). (**c**) and (**d**) Magnified fluorescence images of modified HAR microchannel for COC and PMMA, respectively.

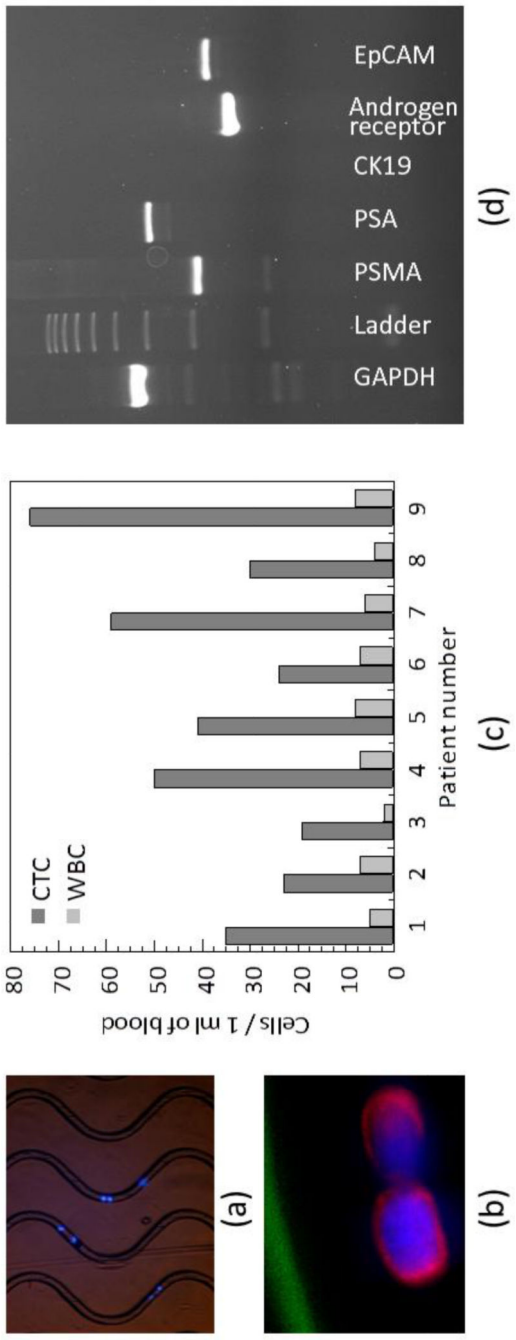

Fig. 7.

Isolation and analysis of CTCs using HT-CTC device. (**a**) Image of MCF7 cells isolated using antiEpCAM modified isolation bed and stained with molecular stain DAPI. (**b**) Fluorescence image of two CTCs isolated from blood secured from patient with prostate cancer. CTCs demonstrated characteristic positive staining for molecular marker DAPI (blue) and cytokeratins (red) and negative staining for CD44. (**c**) Summary of CTC isolation data for patients with prostate cancer. High purity of isolate sample is evident by low numbers of co-isolated leukocytes. (**d**) Results showing the molecular profiling of

EpCAM(+) CTCs. In this case, the total RNA was extracted from the CTCs, with the mRNA reverse transcribed into cDNA using dT primers and then subjected to PCR with the gene specific primers.